Presented at the International Symposium
on Nuclear Collisions and their
Microscopic Description, Bled, Yugoslavia,
September 26 - October 1, 1977

LBL-7164

CONF-770987--4

HIGH ENERGY COLLISIONS OF NUCLEI: EXPERIMENTS

Harry H. Heckman

September 1977

Prepared for the U. S. Department of Energy
under Contract W-7405-ENG-48

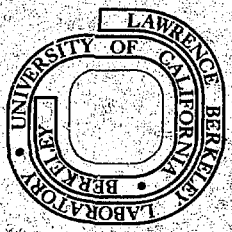

LBL-7164

HIGH ENERGY COLLISIONS OF NUCLEI: EXPERIMENTS

Harry H. Heckman*+

Institut für Kernphysik der J.W. Goethe-Universität, Frankfurt/M.
Lawrence Berkeley Laboratory, Berkeley, California

INTRODUCTION

During the past few years, we have witnessed an expanding and increasingly comprehensive experimental program on the collisions between nuclei at high energy. To date, experiments on the high energy interactions of nuclei have been primarily concerned with the measurements of single particle inclusive spectra in reactions of the type B+T → F+X, where B and T are the beam and target nuclei, F is the detected (single) fragment, and X represents all other undetected particles. For this reason I shall focus my discussion on this class of experiments.

Much of the data I shall present will be expressed in terms of the rapidity variable, $y = \tanh^{-1}\beta_{\parallel}$, where $\beta_{\parallel} = v_{\parallel}/c$ is the longitudinal component of the velocity $\vec{\beta}$ of the produced fragment (F). For non-relativistic velocities, y is simply $\beta_{\parallel}$. The usefulness of the rapidity variable stems from the fact that the Lorentz transformation of the rapidity variable is given by $y' = y+\xi$, where the additive constant ξ, known as the boost parameter, is related to the Lorentz factor $(\gamma = (1-\beta^2)^{-1/2})$ of the transformation by the expression $\xi = \ln(\gamma+(\gamma^2-1)^{1/2})$. The consequence of this property of rapidity is that the shape of any function f(y) is Lorentz invariant. This is schematically shown in Fig. 1, where we show a distribution f(y) as observed near y = 0 (such a distribution could be contours of an invariant cross section for low energy fragments) and f(y'), this same distribution when observed from a moving frame (Lorentz factor = γ). The rapidity distributions f(y) and f(y') have the same shapes, separated by the distance ξ along the rapidity axis.

It is common terminology to describe the collisions between nuclei as being peripheral or central, involving pro-

jectile fragmentation, target fragmentation, etc. In terms of rapidity, these qualitative descriptions can be operationally defined. As indicated in Fig. 1, particles produced with $y \approx 0$ are related to target fragmentation, whereas particles produced with $y \approx \xi \equiv y_{proj}$ (where y_{proj} is the rapidity of the incident projectile nucleus) are identified with the fragmentation products of the projectile. Such fragments are observed to have velocities nearly equal to that of the incident beam. The distributions of the target and projectile fragments are the same in their respective frames. Collisions that give rise to fragments in the regions of $y = 0$ and ξ are said to be peripheral. Central collisions produce fragments that tend to occupy the intermediate region of rapidity, where the fragments cannot be definitely related to either the target or projectile nucleus.

With this general viewpoint in mind, I thought it would be interesting and, hopefully, informative to present this experimental review as a "survey in rapidity space". I shall therefore divide my talk into sections on the target, intermediate and projectile regions of rapidity, emphasizing the production of light nuclei in high-energy heavy ion collisions. My last topic will be a summary of target fragmentation experiments using nuclear emulsion and AgCl visual track detectors.

SURVEY IN RAPIDITY

A) The Target Region

To illustrate the production of fragments at low rapidities, I shall refer to the recently published data of Gosset, et al[1] who have studied the inclusive reactions

$$\begin{matrix} {}^{20}_{4}\mathrm{Ne} \\ \mathrm{He} \end{matrix} + \begin{matrix} \mathrm{U} \\ \mathrm{Al} \end{matrix} \rightarrow F + X$$

at selected beam energies $T_A = 0.25$, 0.40, 2.1 GeV/A. The fragments F detected were protons through nitrogen, produced at angles between $\theta_{lab} = 25^\circ$ and 150° in the energy range $30 \leq T_A \leq 150$ MeV/A. Although this energy range is higher than that usually identified with target (i.e., evaporation-like)

processes, the data exhibit , nonetheless, strong target-related phenomena. The data from this experiment are comprehensive and exemplify well the target, and near-target regions of rapidity.

Figure 2 is a representive plot of the angular dependence of the measured differential cross sections for the production of the hydrogen and helium isotopes in the energy interval $30 \leq T_A \leq 50$ MeV/A in the reaction $^{20}Ne + U \rightarrow F + X$ at beam energy 400 MeV/A. The important features of these data are:

i) The angular distributions are smooth and forward-peaked, tending to an "evaporation peak" at low energies.

ii) The forward-peaking increases with mass of the fragment.

iii) Protons are predominant, particularly in the back hemisphere.

iv) Similar behavior is observed at all other beam energies.

Figure 3 shows the angular dependence of ^3He production on beam energy, the target and projectile masses, and the energy window of the ^3He fragment. If we consider the angular distributions for the energy interval 30 - 50 MeV/A, we arrive at the following qualitative conclusions:

i) As the energy of the ^{20}Ne projectile decreases from 2.1 to 0.4 to 0.25 GeV/A, the angular distribution of the ^3He produced in the reaction $^{20}Ne + U \rightarrow {}^3He + X$ becomes increasingly peaked in the forward direction (curves a,b,c).

ii) At 2.1 GeV/A, the production of ^3He from ^{20}Ne projectiles on U and Al targets (curves a,d) is shown to be sensitive to the target mass, whereas

iii) the production of ^3He (30-50 MeV/A) by ^4He and ^{20}Ne projectiles on U at 400 MeV/A is shown to be independent of the projectile mass (curves b,e).

Similar behavior is observed for the ^{3}He spectra at the higher energy window, 50 - 100 MeV/A, the most notable difference being the increased forward-peaking of the angular distributions. To reiterate, a general feature of fragment production in heavy ion collisions is for increased emission in the forward-hemisphere as a) the beam energy decreases and b) the energy window of the fragment increases.

In Fig. 4 contours of the invariant cross sections $p^{-1}\, d^2\sigma/dEd\Omega$ for the production of ^{3}He fragments in the reaction ^{20}Ne + U → ^{3}He + X are plotted in the rapidity y vs. $p_\perp$ plane, where the transverse momenta are given in MeV/c per nucleon. Each plot corresponds to different bombarding energies as indicated. The heavy contours are identified by the common logarithm of the invariant cross section. The spacing between all contours corresponds to a constant factor in the cross sections

The rapidities y_{proj} are 0.71, 0.89 and 1.84 for beam energies 250 MeV/A, 400 MeV/A and 2.1 GeV/A. The ranges of rapidity $-0.3 \lesssim y \lesssim 0.6$ and transverse momenta $100 \lesssim p_\perp \lesssim 700$ MeV/c/nucleon covered by this experiment largely confine the data to the regions of rapidity about the target ($y \approx 0$). Note that at 2.1 GeV/nucleon, the contours are well separated from $y_{proj} = 1.84$, and the identification of target-related production of ^{3}He is quite clear. At 250 MeV/nucleon, the smaller rapidity gap between the target and projectile ($\xi \equiv y_{proj} = 0.71$) does not allow such clean separation between the target and projectile rapidity regions for the ranges of y and $p_\perp$ measured.

As discussed previously, each contour is invariant with respect to Lorentz transformations, except for a shift along the rapidity axis by an amount equal to the boost parameter ξ. The key point to interpret these contours is to realize that when fragments are emitted isotropically from a unique moving source, the contours will center about the rapidity of a moving source. Clearly the data show that no such unique moving source exists. At the lowest values of $p_\perp$, the apparent sources have rapidities $y(\beta_{\prime\prime}) \lesssim 0.1$. As $p_\perp$ increases, the shifts in the centroids of the contours towards the higher, intermediate rapidities indicate increasing source velocities.

To account for the apparent spectra of velocities of the particle-emitting sources, Westfall et al. introduced the concept of the nuclear fireball[2]. Referring to Fig. 5, the fireball model assumes that the collision between the projectile and target nuclei leads to the "surgically-clean" removal of nucleons from the overlapping volumes of the colliding nuclei. The remnants of the target and projectile (the spectators) remain at rapidities $y \approx 0$ and $\approx y_{proj}$, respectively. The participating nucleons in the overlapping volumes of the projectile and target are assumed to aggregate into an entity called a fireball whose kinematical properties are determined by the assumption that projectile participants transfer all of their momentum to the effective center-of-mass system of all nucleons that form the fireball. The velocity of the resultant fireball thus moves at rapidities intermediate to the target and projectile. In its elementary form, the fireball is assumed to be an equilibrated, non-rotating ideal gas that expands isotropically in its rest frame with a Maxwellian distribution in energy, characterized by a temperature.

Because the kinematics of fireball production depend on the impact parameter b of the Ne + U collision, a spectrum of b-dependent fireball velocities naturally arises from the model, owing to the unequal target and projectile masses. Although this form of the fireball model satisfactorily accounts for the measured proton inclusive spectrum at incident energies of 250 and 400 MeV/nucleon (the model fails to reproduce the trend of the data in the 2.1 GeV/nucleon Ne + U reaction), the production of a unique fireball system characterized only by the impact parameter of the collision cannot be verified by these data alone. A more direct test for this concept of the fireball model will come about when the projectile and target mass are equal. In this case, the fireball velocity β, as well as its characteristic temperature, will be independent of the impact parameter b owing to the inherent symmetry of all collisions.

B) The Intermediate Region

For an exposition of the region of intermediate rapidities

I shall use some very new and preliminary results obtained by Nagamiya et al.[3] on the inclusive proton spectra produced in the reaction $^{20}Ne + {}^{Pb}_{NaF} \rightarrow p + X$, at beam energy T_A = 800 MeV/A. This experiment involves the use of a magnetic spectrometer that can be rotated about the target to obtain data at high transverse momenta $p_\perp$, for production angles between 10^o and 145^o in the laboratory. Proton momenta are measured in the interval $0.4 \lesssim p \lesssim 2.4$ GeV/c, the upper limit being 1.6 times greater than the momentum/nucleon of the incident beam. Particle identification is made by measurements of i) rigidity p/z (momentum per unit charge), ii) rate of energy loss dE/dx, and iii) velocity β(TOF).

Figure 6 is a contour plot of the invariant cross sections $\sigma_I = Ep^{-2}d^2\sigma/dpd\Omega$ in the $(y, p_\perp/m_pc)$- plane for the production of protons by 800 MeV/A ^{20}Ne incident on Pb. The features of the data presented here are similar to that shown in Fig. 4, but with considerable extensions in the ranges of the rapidities and transverse momenta. Well exhibited here is the shift in the centroids of the contours to higher rapidities as $p_\perp/m_pc$ (= $\eta_\perp$) increases. At low $\eta_\perp$, the contours converge to $y \approx 0$, the target rapidity, whereas at the highest values of $\eta_\perp \gtrsim 1$ the contours become symmetric about the average of the target and projectile rapidities $\langle y \rangle = (y_p + y_T)/2$. Such contours are characteristic of collisions between equal mass particles, for which the average effective source velocity is approximately the center of mass velocity β_{CM} for a nucleon-nucleon system. For $\eta_\perp < 1$ the influence of target fragmentation becomes apparent. Protons from the fragmentation of the ^{20}Ne projectile emitted with small $\eta_\perp$ and θ_{lab} were outside the range of measurements, hence no "projectile" peak is indicated at $y_p = 1.23$.

To approximate collisions between nuclei with equal masses, Nagamiya et al. also examined the reaction Ne + NaF → p + X, at T_A = 800 MeV/A. The results are shown in Fig. 7. As expected, the contours of equal values of σ_I show symmetry about $\langle y \rangle = (y_p + y_T)/2 = 0.615$. We have superimposed on these data calculated contours expected for an isotropic distribution in a frame of reference centered at rapidity $\langle y \rangle$. Note that for low values

of y and $\eta_\perp$, when $y \approx \beta_{||}$ and $\eta_\perp \simeq \beta_\perp$, the computed contours of constant energy, hence σ_I, are semi-circles centered about the emitting source.

Strikingly evident, particularly at small $\eta_\perp$, is the non-existence of a unique particle-emitting source. To reproduce the observed shape of the contours of σ_I would require a superposition of a spectrum of sources over a range of rapidities centered about <y>. This result conflicts with the elemental concept of the production of a unique fireball. A promising refinement of the fireball model which yields a mechanism for producing a continuum of "fire-streak" velocities has been introduced by W.D. Myers. (See the paper by M. Gyulassy, this conference, for further discussions on these and other models of high-energy heavy ion collisions.)

C) The Projectile Region

Nuclear fragments with rapidities (velocities) near that of the incident projectile are associated with the fragmentation of the projectile. The process of projectile fragmentation is one that involves small momentum transfers, with cross sections that depend approximately as $A_{targ}^{1/3}$, characteristic of peripheral phenomena. Experiments on the production of high rapidity fragments ($y \approx y_{proj}$) were among the first to be done with relativistic heavy ion beams. For this reason, the principal features of the processes that lead to, and characterize, projectile fragmentation are relatively well understood.

We list below some of the salient features of projectile fragmentation, largely based on the 0-deg. fragmentation of ^{12}C, ^{14}N, and ^{16}O nuclei at 1.05 and 2.1 GeV/A[4,5,6].

a) $y_{frag} \approx y_{proj}$.

b) The longitudinal ($p_{||}$) momentum distributions in the projectile frame are Gaussian-shaped for $p_{||} \lesssim 400$ MeV/c, with deviations evident for $p_{||} > 400$ MeV/c.

c) The rms widths of the longitudinal momentum distributions $\sigma_{p_{||}}$ are typically 50 - 200 MeV/c for all fragment masses.

d) $\sigma_{p_\perp} \approx \sigma_{p_\parallel}$ to within the experimental error of ≈ 10 %.

e) Production angles are highly collimated in the forward direction, with $\Delta\theta \sim \frac{\sigma_{p_\perp}}{p_{beam}} \lesssim 1^o$.

f) The mean value of longitudinal momentum in the projectile frame $\langle p_\parallel \rangle \neq 0$. It is small and negative, i.e. the fragments of the projectile have rapidities slightly less than y_{proj}.

g) $\sigma_{p_\parallel}$ and $\langle p_\parallel \rangle$ are independent of the target mass and beam energy.

h) Production cross sections factor according to $\sigma_{BT}^F = \gamma_B^F \gamma_T$, where

i) γ_B^F is independent of beam energy and targets and

j) γ_T, the target factor, is independent of beam energy, the beam and fragment masses. (The property of factorization of the cross sections appears to fail for light targets, e.g. H and He.)

k) $\gamma_T \approx A_T^{1/4}$ fits the cross section data to ± 10 %.

With this summary in mind, we turn to some recent experimental results on the fragmentation of ^{4}He at 0.4, 1.05 and 2.1 GeV/A that constitute the thesis project of Len Anderson, LBL[7]. The fragmentation reactions studied by Anderson, are

$$^4\text{He} + \begin{matrix} \text{C} \\ \text{Cu} \\ \text{Pb} \end{matrix} \rightarrow \begin{matrix} \text{p} \\ \text{d} \\ ^3\text{H} \\ ^3\text{He} \end{matrix} + \text{x},$$

where the fragment momenta are in the interval $0.5 \leq p \leq 11.5$ GeV/c and the production angles are $0^o \leq \theta_{lab} \leq 12^o$. The major advance in this experiment is the ability to examine light fragment production over a large range of $p_\perp$, permitting excursions into the rapidity regions above and below y_{proj}. I have selected a few figures from Anderson's thesis, principally pertaining to the 2.1 GeV/A-^{4}He data (p = 2.88 GeV/c/A). The first is shown in Fig. 8, which presents the invariant cross sections

$Ed^2\sigma/p^2dpd\Omega$ vs. rapidity for the production of the H and He isotopes at 0-deg in the α + C reaction.

Dominant is the persistance of the projectile velocity, the peaking of the cross sections at y_{proj}, and the separation of the target and projectile rapidity regions. The widths of the rapidity distributions are approximately proportional to A_P^{-1}, i.e., the widths of the distributions in momentum space are approximately equal. All cross sections are of the same order at y_{proj}, with the near equality of the ^{3}H and ^{3}He cross sections being clearly displayed over nearly five orders of magnitude. The proton cross sections exhibit a plateau in the intermediate rapidity region. The d and ^{3}H, ^{3}He cross sections pass through minima at $y \sim 1.2$, then begin to rise toward the target fragmentation peak at $y = 0$.

Figure 9 shows the target dependence of the invariant cross sections vs. y for the 0^o-production of protons at α-beam momentum 2.88 GeV/c/A. For rapidities $(y_{proj} - y) \lesssim 0.25$, the shapes of the cross section vs. y distributions are consistent with target independence, the amplitudes being approximately proportional to $A_T^{1/3}$. For rapidities $(y_{proj} - y) \gtrsim 0.25$, however, the rapidity distributions in the intermediate regions become markedly target dependent.

The transverse momentum distributions of beam velocity protons ($p = p_{beam}/4$) produced in the reaction α + C → p + x are presented as a function of beam momentum in Fig. 10. The $p_\perp$-distributions up to $p_\perp = 0.2$ GeV/c show no momentum dependence of the invariant cross section for beam momenta between 1.75 and 2.88 GeV/c/A (1.05 and 2.1 GeV/A). Close inspection shows that the 0.93 GeV/c/A data are about 15 % lower at the peak, with a sufficiently increased width in the $p_\perp$-distribution to bring all cross sections into equality at $p_\perp \approx 0.2$ GeV/c.

Some of the important conclusions from this ^{4}He fragmentation experiment are the following (not all demonstrated in the foregoing discussion):

a) Limiting fragmentation: Beam-energy independence of the invariant cross sections vs. $p_\parallel$ and $p_\perp$ out to 0.4 GeV/c (projectile frame) is verified for energies 1 - 2 GeV/A.

b) Angular distributions: In the projectile frame, all fragments show forward-backward and forward-transverse asymmetries in the angular distributions. (This result may indicate a difference between the fragmentations of ^{4}He and heavier ^{12}C, ^{16}O nuclei.)

c) Target dependence for proton production: Assuming that $\sigma \propto A_T^n$, the exponent n is found to have the following values:

1) $n \leq 1/3$ for $p_{frag} \approx p_{beam}$ (GeV/c/A) at $p_\perp = 0$

2) $1/3 \lesssim n \lesssim 1$ for $p_{frag} \lesssim 1$ GeV/c at $p_\perp = 0$

3) $1/3 \lesssim n \lesssim 1/2$ for $p_\perp = 0$ to 0.6 GeV/c

TARGET FRAGMENTATION STUDIES IN VISUAL TRACK DETECTORS

Nuclear emulsions and AgCl crystal detectors are well suited for studies of heavy ion interactions because of their inherent ability to detect particles over 4π steradians, their high spatial resolution and broad range of sensitivity to rates of energy loss. Tabulated below are the technical aspects of a series of experiments on the emission of particles from "catastrophic" collisions between high energy heavy ion projectiles and target nuclei in nuclear emulsions (Heckman et al.)[8] and AgCl (Schopper et al.)[9].

Detector:	Emulsions	AgCl
Sensitivity:	$I \gtrsim I_{min}$	$I \gtrsim 8.5\ I_{min}$
Beams:	^{4}He, ^{16}O, ^{40}Ar	^{4}He, ^{12}C, ^{16}O
Energies:	0.2 to 2.1 GeV/A	0.25 to 4.2 GeV/A
Measurements:	i) θ_{lab}	i) θ_{lab}
	ii) dE/dx; $E_{proton} \leq 30$ MeV	ii) dE/dx; $E_{proton} \leq 28$ MeV
	" ≤ 250 MeV	$E_{He} \leq 200$ MeV/A
	iii) Track ranges ≤ 4 mm ($E < 30$ MeV/A)	
Selection Criteria:	No projectile fragments in forward cone, $\theta < 5^o$, 10^o.	Number of prongs
Targets:	AgBr	AgCl

A) The Emulsion Experiment

The data obtained in the emulsion experiment pertain to non-peripheral (central) collisions, i.e. where no beam-velocity fragments are produced in the forward "projectile-fragmentation" cone. The range (momentum) and angle data are fitted by a covariant, non-relativistic Maxwell-Boltzmann distribution. A 2-parameter fit is made to the range and angle data, a 1-parameter fit is made when the data involves angles measurements only.

The essence of the experimental results are shown in Figs. 11 - 15. Figure 11 shows the rapidity distributions for low energy fragments R $\leq$ 4 mm (particle velocities are obtained by use of the range energy relation for protons) for each of the incident projectiles, ^{4}He, ^{16}O and ^{40}Ar at $\approx$ 2 GeV/A. The mean value of $\beta_{||} = \langle y \rangle$ (the effective rapidity of the particle emitting system) is indicated for each distribution as is the standard deviation $\sigma = \sqrt{\tau/M_n}$. To within the errors of the experiment, the values of $\langle y \rangle$ and σ are independent of the projectile mass, the mean of all distributions being consistent with $\langle y \rangle = 0.014 \pm 0.002$ and $\sigma = 0.082 \pm 0.001$, the latter quantity corresponding temperature $\tau = 6.3 \pm 0.2$ MeV/A.

Figures 12 and 13 are examples of the angular distributions observed for fragments with energies $E_p < 31$ MeV and $E_p < 250$ MeV, resp., obtained with $\approx$ 2 GeV/A beam projectiles. Drawn through the data are curves derived from the fitted Maxwellian distributions. The distributions are presented in terms of $dN/d\theta$ and $dN/d\cos\theta$. For the ^{16}O data, the individual fits to the forward and backward hemispheres are also indicated.

Figures 14 and 15 show the angular distributions $dN/d\cos\theta$ vs. $\cos\theta$ for $E_p < 31$ MeV and $E_p < 250$ MeV, respectively, for the lowest beam energy, ^{16}O at 0.20 GeV/A. The notable difference between the ^{16}O-produced fragments at 2.1 and 0.2 GeV/A is the significant increase in the relative production of fragments in the forward hemisphere as the beam energy decreases. The shift of the angular distribution of the low energy fragments $E_p <$ 31 MeV to small r forward angles is due to an increase in $\beta_{||}$ 0.017 to 0.039, while the temperature τ, based on the results

of the $R \leq 4$ mm data, remains essentially constant, i.e. 5.3 to 6.2 MeV/A. For energies $E_p < 250$ MeV, the distribution of fragments produced by 0.20 GeV/A ^{16}O is increasingly peaked forward, indicated by the fact that $\chi_o \equiv \beta_{||} / \sqrt{2\tau/M_p}$ increases from 0.26 to 0.62 as the beam energy decreases from 2.1 to 0.20 GeV/A.

Some general conclusions of the experiment, some of which are based on a more detailed analysis of the data, are:

1) There is no unique particle-emitting system, characterized by a center-of-mass velocity $\beta_{||}$ and spectral velocity $\beta_o = \sqrt{2\tau/M_n}$, that accounts for the spectra of fragment ranges (momenta) and angles.

2) The dN/dθ distributions are broad, Maxwellian-like, with maxima that shift toward smaller angles as the fragment energy increases, and as beam energy decreases.

3) For each fragment energy range $E_p < 30$ and $E_p < 250$ MeV, the changes in the angular distributions are primarily due to increased forward-coning of the angles in the forward hemisphere. The respective angular distributions in the backward hemispheres are essentially invariant with respect to beam and energy.

4) No statistically significant structure, attributable to well-defined collective phenomena, is observed in the range or angular distributions.

B) The AgCl Experiment

The angular distributions dσ/dθ of fragments with ionization rates $I \gtrsim 8.5\ I_{min}$ emitted from stars with prong numbers $n \geq 8$-16 produced by ^{12}C and ^{16}O projectiles, T_A = 0.25, 0.87 and 2.1 GeV/A, in AgCl detectors are shown in Fig. 16. The curves that are shown on each distribution are the expected angular distribution of the low-energy, evaporation particles (based on Le Couteur's theory), fitted by χ^2-methods to the data.

Figure 17 augments the data shown in Fig. 16 by including two additional spectra, taken with ^{12}C at 1.7 and 4.2 GeV/A. The data are also presented as histograms with statistical errors.

The conclusions one can make from the data shown in Figs. 16 and 17 are that i) the angular distributions in the backward hemispheres are satisfactorily accounted for by an evaporation-like spectrum, and that the shapes of the spectra $\theta_{lab} > 90^{o}$ do not depend sensitively on the beam energy; ii) The general trend of the spectra is to show an increased forward-peaking as the energy of the projectile decreases from 2.1 to 0.25 GeV/A — an observation first made by the Frankfurt Group on the basis of these AgCl experiments and attributed to density effects in nuclear matter.

These results are, therefore, in general agreement with the various data I have presented. In particular, the emulsion and AgCl results both show that the angular distribution for fragments with energies $\lesssim$ 30 MeV emitted at $\theta_{lab} > 90^{o}$ are nearly independent of projectile and energy, consistent with a Maxwellian distribution. The essential difference between the experiments is the significant excess of particles observed at forward angles in the AgCl experiment, not evident in the emulsion data.

At the Fall Creek Falls Meeting[9], Schopper interpreted the peaks in the $d\sigma/d\theta$ distributions observed in AgCl detectors to be due to a superposition of (predominantly) two spectra: 1) A "background" spectrum of low-energy fragments, mainly protons with energies $\lesssim$ 28 MeV. This spectrum appears to change little with beam and energy. 2) A spectrum of He particles, whose angular distribution exhibits much more forward peaking owing to (see Figs. 2 and 3) a) their increased mass and b) their higher energies (recall that He nuclei are detected up to 200 MeV/A in AgCl).

To demonstrate this, Schopper obtained an expected angular distribution of ^{4}He nuclei $\leq$ 200 MeV/A by applying the measured cross sections for Z = 1 and Z = 2 fragments of Cosset et al.[1], Fig. 2, to the calculated angular distribution given by the intranuclear cascade calculations of Smith and Danos[10]. Normalizing this calculated He spectrum to the fitted evaporation spectrum, Schopper obtained the results shown in Fig. 18.

Here, the observed angular distribution of fragments produced by ^{16}O at 0.87 GeV/A is fitted to an evaporation spectrum. The computed, normalized He spectrum, represented by the dark circles, is also shown in this figure. Adding the He distribution to the evaporation spectrum yields the angular distribution identified by the dashed curve.

The hypothesis that the angular distributions of fragments measured in AgCl detectors are composite spectra of H and He nuclei, each with characteristically different energy ranges, is realistic. The changes in the angular distributions with beam energy thus would be attributable to shifts in the He distributions relative to the more nearly energy-independent proton spectra. The important task now is to carry out experiments with both AgCl and emulsion detectors to identify He fragments and to establish their beam-energy dependent angular distributions.

REFERENCES

* Permanent address: Lawrence Berkeley Laboratory, Berkeley CA, 94720, USA.

† Alexander von Humboldt Award, 1977-78.

1. J. Gosset, H.H. Gutbrod, W.G. Meyer, A.M. Poskanzer, A. Sandoval, R. Stock, and G.D. Westfall, Phys. Rev. C 16, 629 (1977).

2. G.D. Westfall, J. Gosset, P.J. Johansen, A.M. Poskanzer, W.G. Meyer, H.H. Gutbrod, A. Sandoval, and R. Stock, Phys. Rev. Letters 37, 1202 (1976).

3. S. Nagamiya, private communication, 1977.

4. H.H. Heckman, D.E. Greiner, P.J. Lindstrom, and F.S. Bieser, Phys. Rev. Letters 28, 926 (1972).

5. D.E. Greiner, P.J. Lindstrom, H.H. Heckman, B. Cork, and F.S. Bieser, Phys. Rev. Letters 35, 152 (1975).

6. P.J. Lindstrom, D.E. Greiner, H.H. Heckman, B. Cork, and F.S. Bieser, LBL Report 3650 (1975).

7. L. Anderson, thesis (in preparation) and private communication, 1977.

8. H.H. Heckman, H.J. Crawford, D.E. Greiner, P.J. Lindstrom, and L.W. Wilson, Proceedings of Meeting on Heavy Ion Collisions, Fall Creek Falls State Park, TN, June 13-17, 1977.

9. E. Schopper, H.G. Baumgardt, and E. Obst, Proceedings of Meeting on Heavy Ion Collisions, Fall Creek Falls State Park, TN, June 13-17, 1977.

10. R.K. Smith and M. Danos, Proceedings of Meeting on Heavy Ion Collisions, Fall Creek Falls State Park, TN, June 13-17, 1977.

This work was done with support from the U. S. Department of Energy.

FIGURES AND FIGURE CAPTIONS

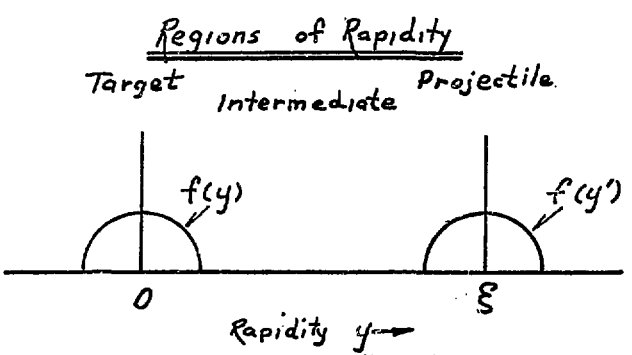

Fig. 1. Target and projectile fragmentation regions are identified with regions of rapidity, $y = \tanh^{-1} \beta_{||}$, about $y \approx 0$ and $y \approx \xi = y_{proj}$, respectively. Fragments with intermediate rapidities lie between the target and projectile distributions.

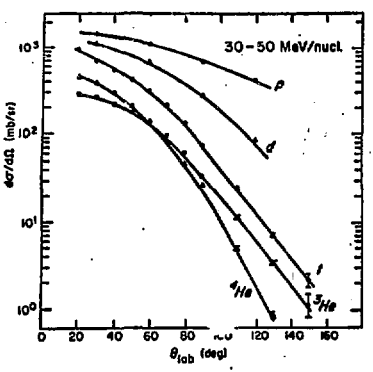

Fig. 2. Angular distributions for the light fragments produced in the interaction of ^{20}Ne with U at 400 MeV/nucleon, integrated over the velocity window from 30 to 50 MeV/nucleon.

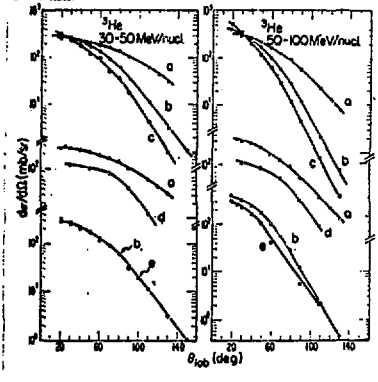

Fig. 3. Cross comparison of angular distributions of ^{3}He fragments integrated for two velocity windows at different incident energies and for different projectiles and targets: (a)-(c) Ne on U at 2.1, 0.4, and 0.25 GeV/nucleon, resp.; (d) Ne on Al at 2.1 GeV/nucleon (raised by a factor of 10); and (e) ^{4}He on U at 0.4 GeV/nucleon (raised by a factor of 10).

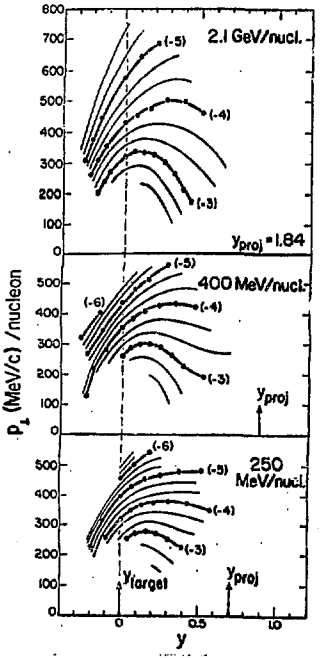

Fig. 4. Contours of constant invariant cross sections in the $(y,p_\perp)$ plane for ^{3}He fragments from ^{20}Ne on U at different bombarding energies.

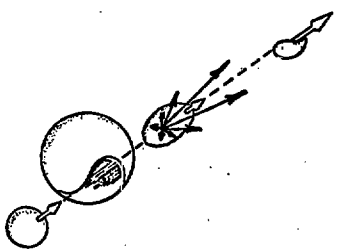

Fig. 5. Schematic illustration of the fireball model.

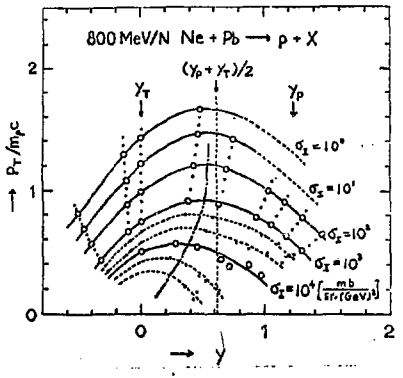

Fig. 6. Contours of constant invariant cross sections in the $(y, p_\perp/m_pc)$ plane for the production of protons from 800 MeV/A ^{20}Ne on Pb.

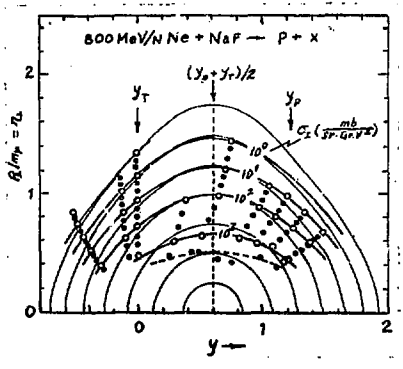

Fig. 7. Contours of constant invariant cross sections in the $(y, p_\perp/m_pc)$ plane for the production of protons from 800 MeV/A ^{20}Ne on NaF. Thin lines are for an isotropic distribution centered at $\langle y \rangle = 0.61$.

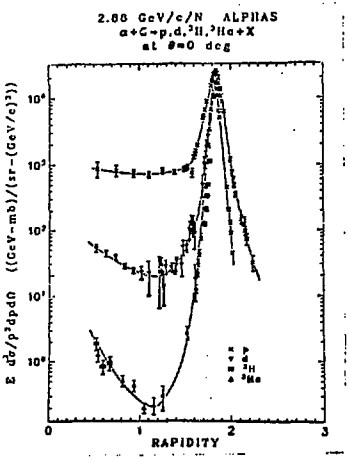

Fig. 8

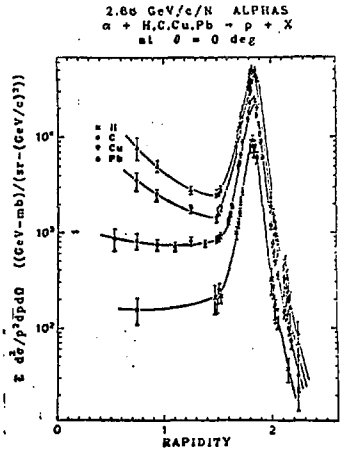

Fig. 9

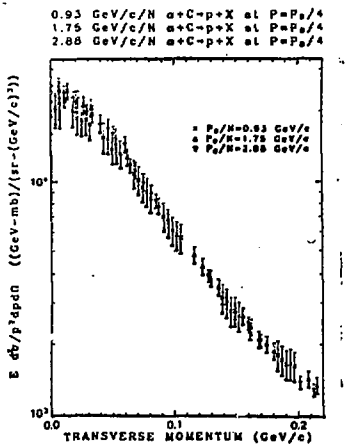

Fig. 10

Fig. 8. Invariant cross sections vs. rapidity for the production of p, d, ^{3}H and ^{3}He at $\theta_L = 0^o$ from 2.1 GeV/A ^{4}He incident on ^{12}C.

Fig. 9. Target dependence of invariant cross sections for the production of protons at 0^o, 2.1 GeV/A ^{4}He on H, C, Cu and Pb.

Fig. 10. Transverse momentum distributions of beam velocity protons from the reaction α + c → p + x as a function of beam momentum.

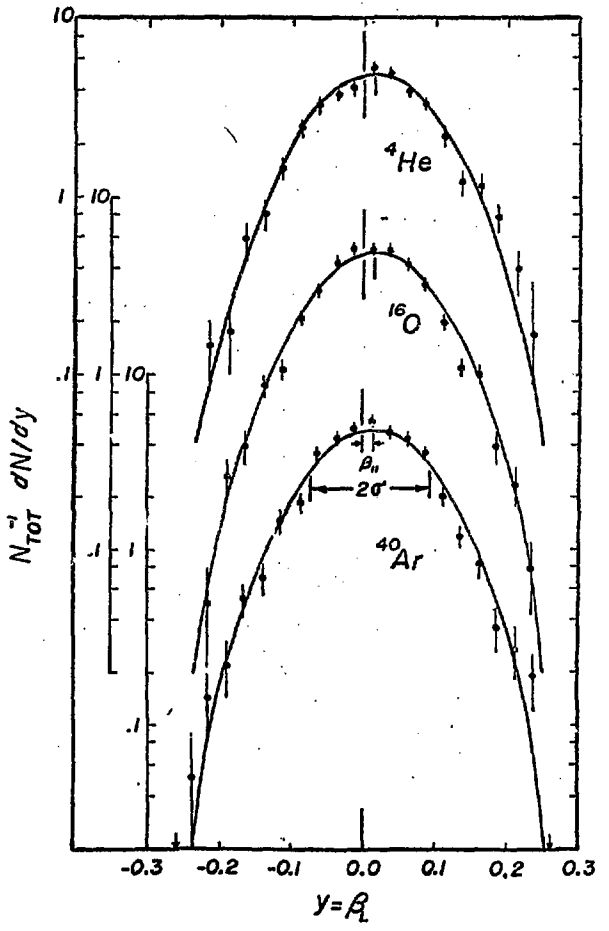

Fig. 11. Rapidity distributions for fragments with ranges R < 4 mm (30 MeV/A). Cut-off values are indicated by arrows on the abscissa. Also indicated are the mean rapidities β_{II} = <y> and the standard deviations $\sigma = \sqrt{\tau/m_p}$. Projectile energies are ≈ 2 GeV/A.

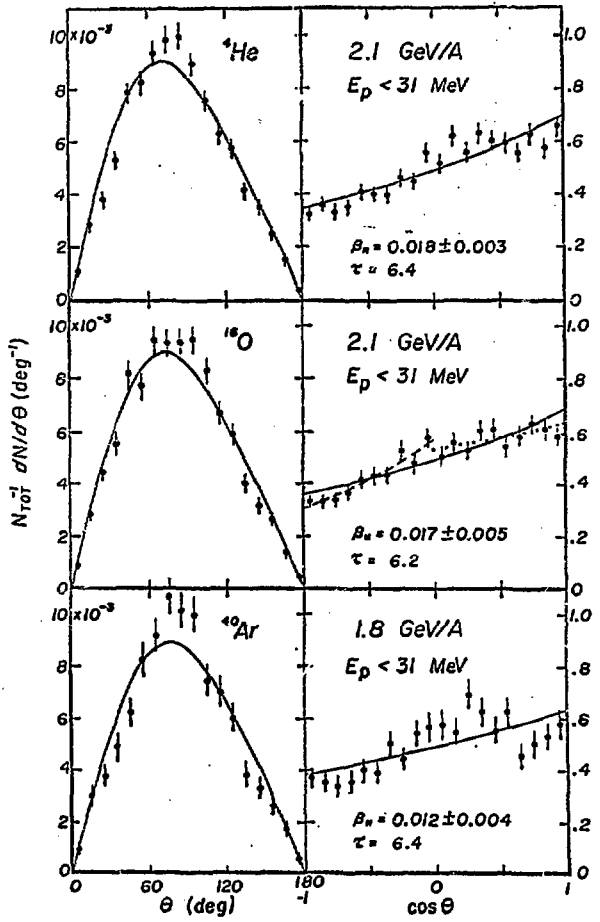

Fig. 12. Angular distributions for fragments, E_p < 31 MeV. Projectile energies at ~ 2 GeV/A. Solid curves are fits of the data, using the parameters indicated. The dashed and dotted curves are fits to the data, for the backward and forward hemispheres, respectively.

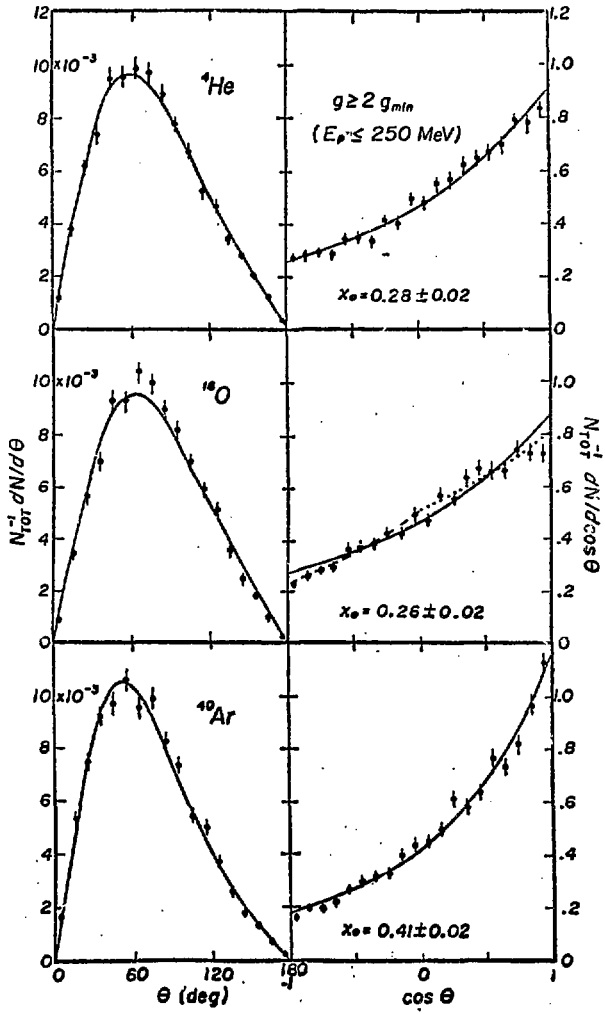

Fig. 13. Angular distributions for fragments E_p < 250 MeV. See caption Fig. 12 for identification of the plotted curves.

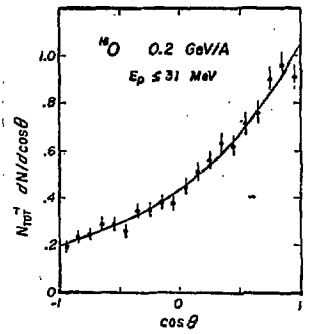

Fig. 14. Angular distribution dN/dcosΘ vs. cosΘ for fragments, E_p < 31 MeV. Projectile nucleus is ^{16}O at 0.2 GeV/A. The parameters of the fitted curve are $\beta_{\parallel}$ = 0.039 and τ = 5.3 MeV/A.

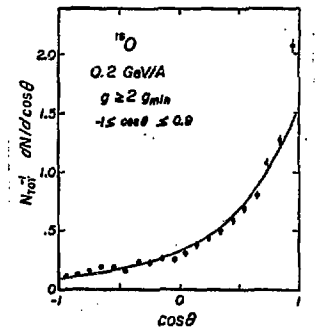

Fig. 15. Angular distribution dN/cosΘ vs. cosΘ for fragments E_p < 250 MeV. Projectile nucleus is ^{16}O at 0.2 GeV/A. The parameter for the fitted curve is χ_o = 0.62. The data point at cosΘ = 0.9 was not included in the fit, owing to a background of Z = 1 fragments of the projectile not excluded by our selection criteria.

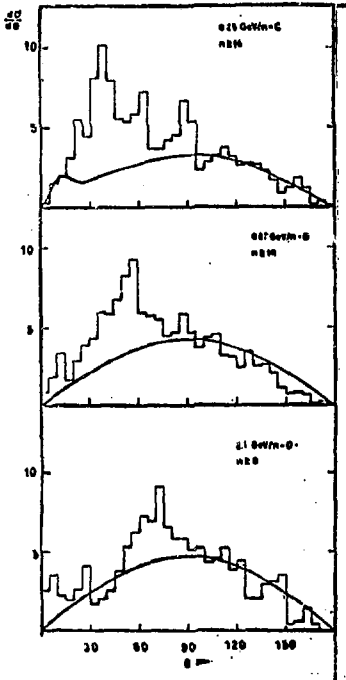

Fig. 16. Angular distributions dσ/dΘ for fragments observed in AgCl detectors. Curves are fitted evaporation component.

Fig. 17. Histograms, with assigned errors, of the angular distributions of fragment production in AgCl detectors. Projectiles are ^{12}C and ^{16}O, with energies 0.25 to 4.2 GeV/A.

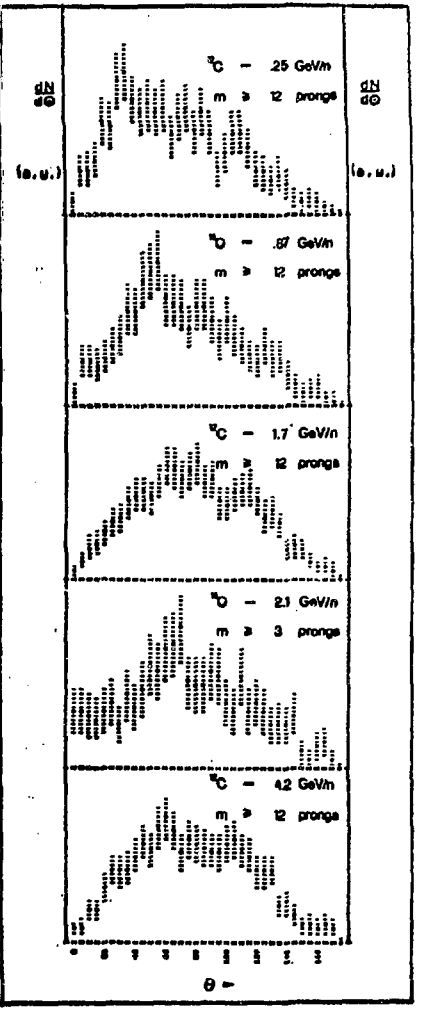

Fig. 17

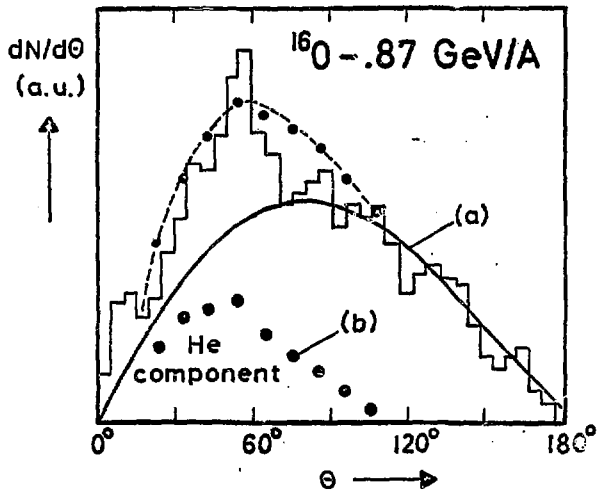

Fig. 18. Ideograms of fragment angular distributions in AgCl with composite angular distributions (a) the fitted evaporation spectrum, $E_{proton} < 28$ MeV and (b) the computed He spectrum, $E_{\alpha} < 200$ MeV/A, based on Refs. 1 and 10. Sum of (a) and (b) is shown as dashed line.